A Novel DWT-based Method for Image Sharpness Measure using Edge-related Frequency Components

Yuan-Kang Lee
Communication Engineering
National Taiwan University
Taipei, Taiwan
r12942062@ntu.edu.tw

Jian-Jiun Ding
Communication Engineering
National Taiwan University
Taipei, Taiwan
jjding@ntu.edu.tw

Abstract— **In this paper, a novel no-reference image quality metric of sharpness is proposed. Our image quality metric is evaluated on two key attributes discerned during the assessment of image sharpness by the human visual system (HVS): 1. Image sharpness is principally contingent upon the salience of edges within the image. 2. With an increase in the decomposition level of the Discrete Wavelet Transform (DWT), the high-frequency coefficients correspond to higher spatial frequency information in an image. Experimental results show that in comparison to other state-of-the-art metrics, our method not only accurately assesses image sharpness in both defocus and motion blur scenarios but also showcases superior precision and broader applicability.**

Keywords—Image sharpness, image blur, no-reference, discrete wavelet transform, edge detection, image quality assessment

I. INTRODUCTION

As the development of digital cameras, augmented reality (AR), virtual reality (VR), autonomous vehicles, and medical imaging systems advance rapidly, the precise evaluation of the image sharpness is essential in the fields of image processing and computer vision. A high-quality image characterized by high sharpness contains fine details and textures, enriching the overall viewing experience while also augmenting precision in content analysis. As subjective methods for assessing image sharpness are time-consuming and inconsistency, objective assessments have taken precedence as the primary focus of research. The evaluation of image sharpness aims to analyze the clarity of the acutance and the texture in an image, serving as an important metric in tasks such as image deblurring [1][2], auto-focus algorithms [3][4][5], and remote sensing image analysis [6]. Broadly, objective methods for evaluating image sharpness can be categorized into three types: full-reference image quality assessment (FR-IQA), reduced-reference image quality assessment (RR-IQA), and no-reference image quality assessment (NR-IQA). FR-IQA involves comparing an image to a high-quality reference image, while RR-IQA relies on partial information from a reference image. On the other hand, NR-IQA evaluates image quality without any reference image. In practical applications, obtaining an undistorted reference image is frequently unfeasible. Hence, NR-IQA has emerged as the predominant development focus in contemporary image quality assessment endeavors.

In current research on no-reference evaluation of image sharpness, spatial-domain methods and transform-domain are widely employed. Spatial-domain methods are based on the concept that when an image is affected by blur, its contrast decreases, and its edges weaken. Utilizing the spatial property, many methods use the image's gradients and edge strength to assess image sharpness [7][8]. Due to the maturity of current image edge detection methods [9][10][11], employing spatial-domain techniques for image sharpness assessment is intuitive and straightforward. Transform-domain methods primarily use transform techniques such as the Discrete Fourier Transform [12], the Discrete Cosine Transform [13], and the Discrete Wavelet Transform [14][15] to extract the image's frequency components. Generally, the high-frequency components within an image its level of detail. When the image suffers from blurring, the high-frequency elements significantly diminish. Consequently, a blurred image contains less high-frequency information than a sharp image. Yet, both spatial-domain and transform-domain approaches are susceptible to the influence of noise in accessing image sharpness. Moreover, we observed that the existing no-reference image sharpness metrics can evaluate defocus blur but struggle to accurately assess cased of motion blur. The limitation results in a current lack of a more widely applicable metric for measuring image sharpness.

In our work, a novel no-reference metric for measuring image sharpness is proposed. Our method is based on two primary properties of the HVS regarding image sharpness:

1. The high-frequency elements associated with edges in images are the most significant factors used by human eyes to assess the image sharpness.
2. The DWT at different decomposition levels captures various scales of image's high-frequency coefficients in the transform domain. As the level of decomposition increases, the obtained high-frequency coefficients correspond to the information of higher spatial frequency in an image.

The proposed image sharpness metric leverages the edge-related DWT coefficients and combine three different scales of high-frequency components, culminating in a final sharpness map. As blur predominantly affects high-frequency elements, the low-frequency components of an image remain relatively unchanged. Hence, our metric relies on the content of edge-related and weighted high-frequency coefficients in the final sharpness map relative to its low-frequency components. The rest of this paper is structured as follows. Section II present the analysis of our metric. Section III shows the performance of our method compared to other state-of-the-art metrics in different experiments. Section IV offers conclusions of our work.

II. PROPOSED IMAGE SHARPNESS MEASURE

Defocus blur and notion blur are two types of blurring that can significantly degrade image quality. Defocus blur occurs when the camera lens fails to focus properly on the target, resulting in a global blur across the entire image. On the other hand, motion blur arises due to the relative movement between the camera and the object during image capturing, resulting in a directional blurred smudges in the image. The characteristic of defocus blur causing a uniform blur across the image makes it relatively easier for blur evaluation. Compared to defocus blur, the image influenced by motion blur exhibits a distinct property: a noticeable decrease in the high-frequency energy along the direction of motion in the blurred image [16][17][18]. Due to the different effect of motion blur and defocus blur on images, solely employing spatial or transform domain methods is ineffective for accurately evaluating sharpness.

A. Combination of the Spatial and the Transform Information

The two-dimensional DWT decomposes an image into 4 divided layers, and a DWT decomposition result with multiple decomposition levels is shown in Fig 1.

1. LL layer: Represents low-frequency components of the image, which remain relatively unchanged during blurring.
2. LH layer and HL layer: Capture image's high-frequency components along horizontal and vertical directions, both effected noticeably by blurring.
3. HH layer: Contains high-frequency elements along the diagonal direction, also dramatically effected by blurring.

To align our proposed metric more closely with the human visual assessment of image sharpness, we employ Sobel edge detection method on the LL layer to extract high-frequency coefficients related to edges. Through this approach, we not only enhance the significant influence of edges on sharpness but also reduce the impact of noise on sharpness evaluation. Since the Haar transform holds higher practical value because of its computational efficiency and implementation simplicity compared to other wavelet transforms, we then apply the Haar transform to capture edge-related high-frequency coefficients. In our method, the edge map *EM* is expressed as in (1).

$$EM_i = \sqrt{LH_i^2 + HL_i^2 + HH_i^2} \cdot EdgeMask \qquad (1)$$

The sub-bands *LH*, *HL*, and *HH* are generated through the Haar transform's decomposition process, and the lowercase notation *i* denotes the decomposition level. *EdgeMask* denotes the outcome of edge detection achieved by applying the Sobel operator to the LL layer of the image. The improved edge map include all high-frequency elements corresponded to edges. It is worth noting that to encompass all edge-related coefficients, an edge dilation operation becomes necessary. We employ a dilation process on *EdgeMask*, which expands the size of the edges fourfold, facilitating the inclusion of various scales of high-frequency coefficients related to edges.
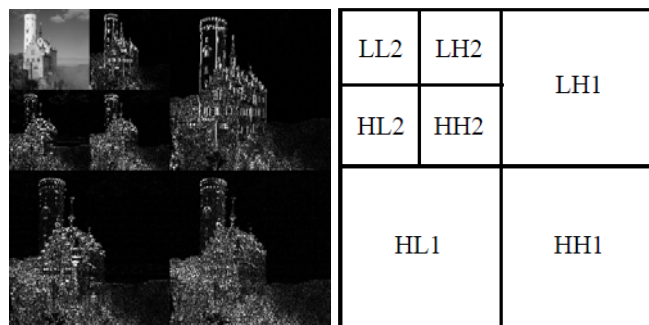

Fig. 1 A DWT decomposition result with multiple decomposition levels

B. Spatial Frequency and DWT Coefficients

Our human visual system assesses image sharpness based on the image's spatial frequency. An image with higher spatial frequency exhibits sharper edges, characterized by shorter rise distance. The rise distance of an edge can be expressed as the difference of pixel levels between 10% to 90% of its final value. Fig. 2(a) shows two bar pattern with different spatial frequencies. The upper half displays a high-quality bar pattern with high spatial frequency, while the lower half shows a quality-degraded bar pattern with low spatial frequency. Fig. 2(b) illustrates two edge with high and low spatial frequencies.
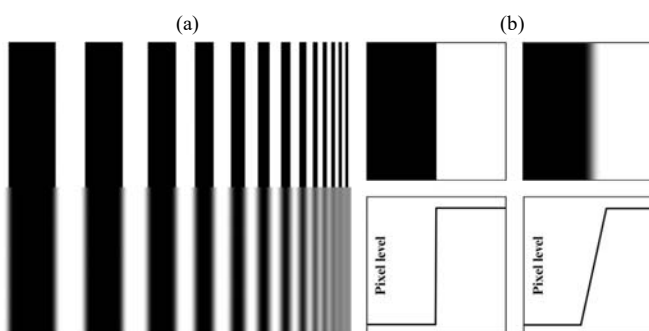

Fig. 2(a) The comparison of bar pattern images exhibiting different spatial frequencies. Fig. 2(b) The top left corner: the edge image with high spatial frequency. The bottom left corner: the pixel level variation curve of the edge with high spatial frequency. The top right corner: the edge image with low spatial frequency. The bottom right corner: the pixel level variation curve of the edge with low spatial frequency.

There are numerous well-established and widely applied methods in the industry for computing spatial frequencies in images [19][20][21]. Yet, these methods require specific test charts such as the slanted-edge chart [19], the Siemens star chart [20], and the dead leaves chart [21] to be captured by a camera for the spatial frequency measurement. This limitation restricts their applicability, rendering these methods unsuitable for evaluating sharpness across various scenes. To enhance the applicability of sharpness evaluation, the pivotal focus lies in extracting higher spatial frequency information from image's content. Our study revealed that the high-frequency elements extracted by higher decomposition levels contain information of higher spatial frequency. To verify this image characteristic, we utilize the Power Spectrum Density (PSD) to analyze the spatial frequency information of an image. PSD represents the

ISSN 2464-4617 (print)
ISSN 2464-4625 (online)

Computer Science Research Notes - CSRN 3401
http://www.wscg.eu

WSCG 2024
POSTERS

distribution of energy across different spatial frequencies in the image. It is obtained through the Fourier transform of the image, providing insight into the frequency content and spatial characteristics. For an image f(m,n) with dimensions of M x N pixels, its Fourier Transform F(u,v) is represented as shown in (2). PSD can then be expressed as in (3).

$$F(u, v) = \sum_{m=0}^{M-1} \sum_{n=0}^{N-1} f(m,n) e^{-j2\pi(um/M+vn/N)} \quad (2)$$

$$P(u, v) = 10 \cdot log(|F(u,v)|^2) \quad (3)$$

If an image contains higher spatial frequency information, its mean value of Power Spectral Density (PSD) tends to be higher. To analyze this property, we captured six Siemens star charts with varying levels of sharpness for experimentation. Siemens star charts encompass spatial frequency information ranging from low to high. The Modulation Transfer Function (MTF) for each of these six test charts was calculated using professional image quality software iQ-analyzer to evaluate the image spatial resolution. Fig. 3 displays the Siemens star chart images arranged from left to right in ascending order of sharpness. To quantify the sharpness of these six Siemens star chart images, we utilized MTF50 value, which represents the Modulation Transfer Function at 50% contrast. Table I shows the MTF50 values alongside the mean values of PSD for the edge maps EM1, EM2, and EM3 corresponding to the six Siemens star charts. Experimental data validates that the edge map EM with a higher wavelet decomposition level contains higher spatial frequency information. To enhance the precision of our proposed image sharpness measure, it is imperative to incorporate edge maps at higher decomposition levels. In other words, a comprehensive image sharpness metric necessitates the consideration of finer details in the evaluation.

TABLE I. MTF50 AND MEAN PSD VALUES OF EDGE MAP EM1, EM2, AND EM3 OF SIEMENS STAR CHART IMAGES SHOWN IN FIG .3 (A)-(F)

	Fig .3(A)	Fig .3(B)	Fig .3(C)	Fig .3(D)	Fig .3(E)	Fig .3(F)
MTF50 (LP/PH)	415	461	485	509	521	574
EM$_1$ mean PSD (dB)	50.4666	52.0948	53.4735	54.2395	55.4626	56.0850
EM$_2$ mean PSD (dB)	62.5617	64.1274	65.6600	66.5087	67.4256	68.7728
EM$_3$ mean PSD (dB)	72.5062	74.4403	75.5845	76.5072	77.3337	77.9862

The final edge map EM_f is expressed as in (4), where EM_1, EM_2, and EM_3 represent the edge maps corresponding to the wavelet decomposition level 1, 2, and 3, respectively. It is noteworthy that EM_1 is twice the size of EM_2, and EM_2 is twice the size of EM_3. Hence, for precise generation of the weighted edge map, both EM_1 and EM_2 should be resized to match the dimensions of EM_1.

$$EM_f = EM_1 + EM_2 + EM_3 \quad (4)$$

C. Image Sharpness Evaluation Model

Considering the limited impact of blurriness on the low-frequency components of an image, the assessment of image sharpness relies on the ratio of high-frequency content to low-frequency content. Based on this concept, our proposed image sharpness evaluation model is expressed as in (5), (6), and (7).

$$\overline{EM_f} = \left[\sum_{i=1}^{M/8} \sum_{j=1}^{N/8} EM_f(i,j) \right] / (MN/64) \quad (5)$$

$$\overline{LL_1} = \left[\sum_{i=1}^{M/2} \sum_{j=1}^{N/2} EM_f(i,j) \right] / (MN/4) \quad (6)$$

$$HFEM = \overline{EM_f} / \overline{LL_1} \quad (7)$$

HFEM, EM_f, and LL_1, are denoted as the proposed image sharpness measure using High-Frequency Edge Map, the final edge map, and the low-frequency sub-band decomposed by the level 1 Haar transform, respectively.

III. EXPERIMENTS

We conducted a comparative analysis of our proposed no-reference image quality metric for sharpness HFEM against existing state-of-the-art approaches: CPBD [22], PSI [23], and MGVG [8]. Four sharpness evaluation method were validated using Kodak24 database.

A. Gaussian Blur experiments

We experimented blurring simulations using Gaussian Blur on the images, varying the standard deviation of Gaussian blur from 0.5 to 10 in intervals of 0.5. Several blurred images with varying degrees are shown in Fig .4, using the Kodak8 image. With an increase in the standard deviation, a corresponding decrease in the image sharpness measure is anticipated.
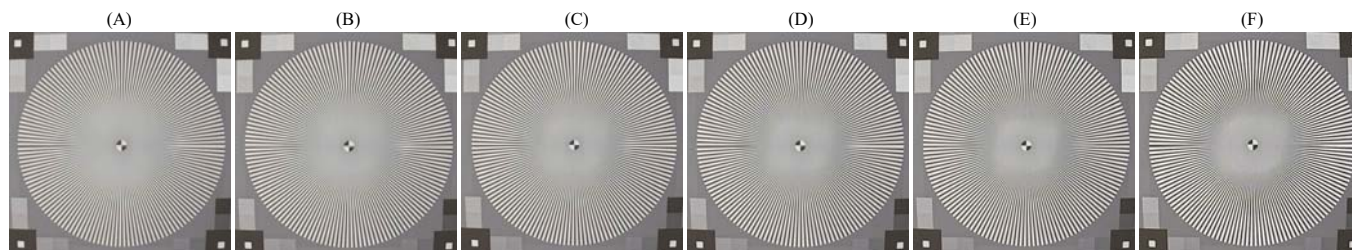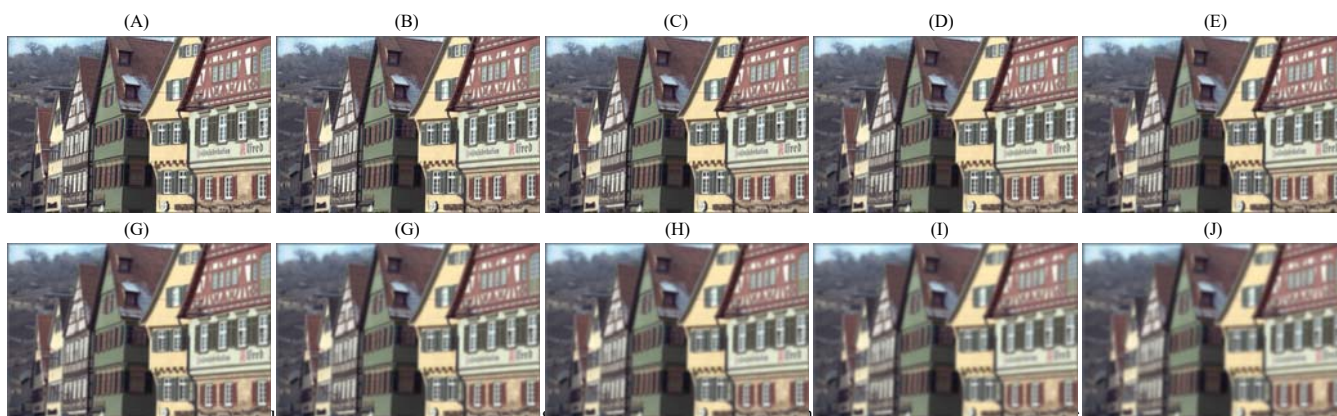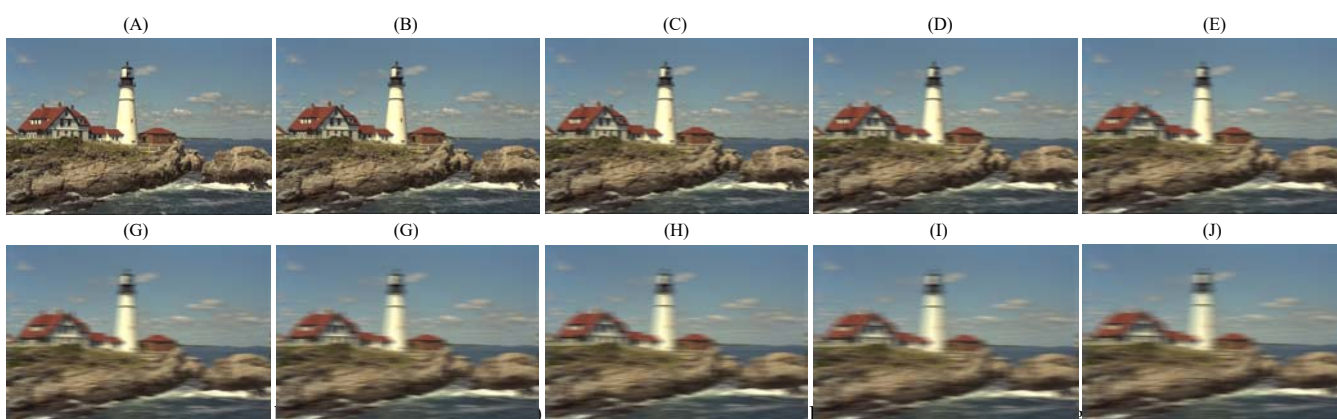

Fig. 3 Siemens star chart contains low and high spatial frequency information. Images (A) - (F) arranged from left to right in increasing order of sharpness.

(A)   (B)   (C)   (D)   (E)

(G)   (G)   (H)   (I)   (J)

Gaussian blur with standard deviations ranging from 0.5 to 4.5, in increments of 0.5. We use Gaussian blur to simulate the impact of defocus on the image.

(A)   (B)   (C)   (D)   (E)

(G)   (G)   (H)   (I)   (J)

blur with varying the motion blur length from 5 to 45, in increments of 0.5. We use motion blur to simulate the impact of motion on the image.

Fig. 6, Fig. 7, Fig. 8, and Fig. 9 illustrate the trend lines of CPBD, PSI, MGVG, and our metric HFEMS. Experimental results show that CPBD and PSI both exhibit inaccuracies in evaluating sharpness if the standard deviation of Gaussian blur exceeds 3. Our proposed metric HFEMS demonstrates great evaluation performance regardless of whether the standard deviation of Gaussian blur is low or high.

B. Motion Blur experiments

Motion blur can be modeled by two parameters: length and angle. The length specifies the quantity of pixels displaced due to camera movement, while the angle determines the direction along which the blur occurs. We experimented motion blur simulations on images, varying the motion blur length from 5 to 100 in intervals of 5. Several blurred images with varying motion-blurred lengths at 0 angle are shown in Fig .5, using the Kodak21 image. With an increase in the motion-blurred length, a corresponding decrease in the sharpness measure is anticipated. Fig. 10, Fig. 11, Fig. 12, and Fig. 13 illustrate the trend lines of CPBD, PSI, MGVG, and our metric HFEMS. Our metric exhibits exceptional and superior performance in evaluating image sharpness. Other existing metrics lack the capability to accurately measure the effect of motion blur.
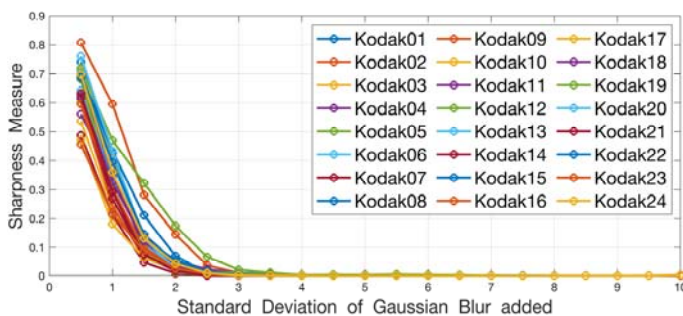

Fig. 6 The variation of CPBD [22] vs Gaussian Blur on Kodak 24 images
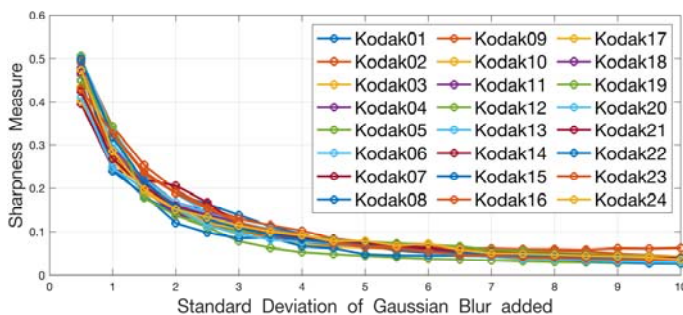

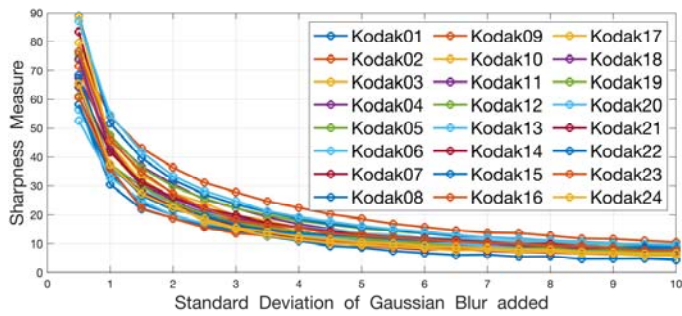Fig. 7 The variation of PSI [23] vs Gaussian Blur on Kodak 24 images

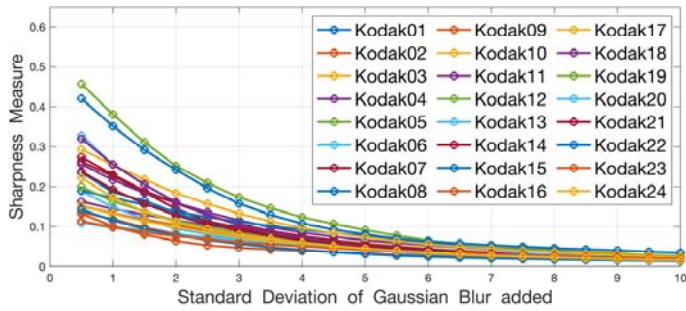Fig. 8 The variation of MGVG [8] vs Gaussian Blur on Kodak 24 images

Fig. 9 The variation of HFEM vs Gaussian Blur on Kodak 24 images

IV. CONCLUSION

In this paper, we propose a novel no-reference image quality metric for evaluating sharpness using High-Frequency Edge Map HFEM. Our approach utilizes both spatial and transform domain information in an image to achieve precise image sharpness measurements. By integrating the concept of the relationship between the decomposition levels of the wavelet transform and the spatial frequency and our method aligns with the Human Visual System. Additionally, our proposed metric accurately assesses the impact of motion blur on the image, surpassing other state-of-the-art image sharpness metrics. In the future, our aim is to utilize this proposed image sharpness metric for the development of a new blind image deblurring method and a camera auto-focus algorithm.

REFERENCES

[1] Leclaire, Arthur, and Lionel Moisan. "No-reference image quality assessment and blind deblurring with sharpness metrics exploiting fourier phase information." Journal of Mathematical Imaging and Vision 52 (2015): 145-172.

[2] Xiang, Xinguang, Hao Wei, and Jinshan Pan. "Deep video deblurring using sharpness features from exemplars." IEEE Transactions on Image Processing 29 (2020): 8976-8987.

[3] Yao, Yi, et al. "Evaluation of sharpness measures and search algorithms for the auto-focusing of high-magnification images." Visual Information Processing XV. Vol. 6246. SPIE, 2006.

[4] Yousefi, Siamak, M. Rahman, and Nasser Kehtarnavaz. "A new auto-focus sharpness function for digital and smart-phone cameras." IEEE Transactions on Consumer Electronics 57.3 (2011): 1003-1009.

[5] Zhang, Zheng, et al. "Focus and blurriness measure using reorganized DCT coefficients for an autofocus application." IEEE Transactions on Circuits and Systems for Video Technology 28.1 (2016): 15-30.

[6] Chen, Guobin, and Maotong Zhai. "Quality assessment on remote sensing image based on neural networks." Journal of Visual Communication and Image Representation 63 (2019): 102580.
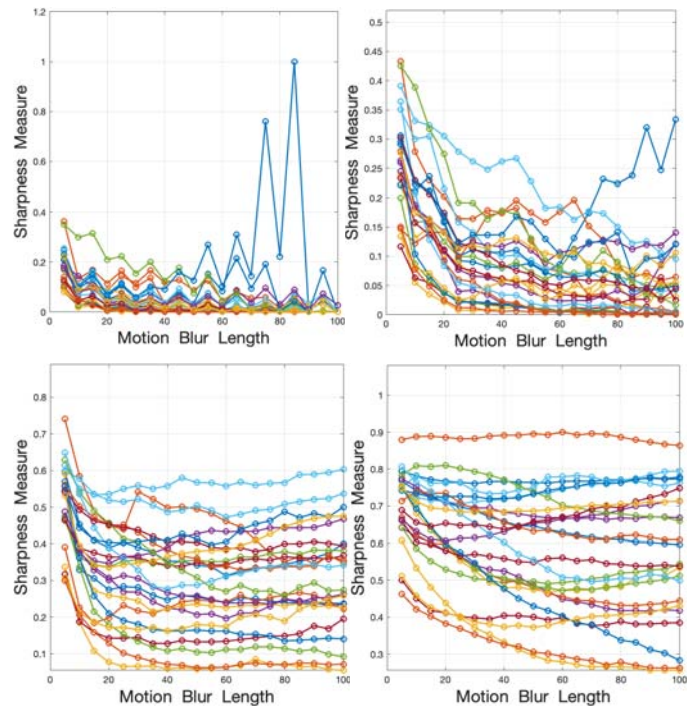
Fig. 10. Trend lines comparison: the variation of CPBD [22] vs motion blur on Kodak 24 images. The top left corner: trend with a motion blur angle 0°. The top right: trend with a motion blur angle 30°. The bottom left: trend with a motion blur angle 60°. The bottom right: trend with a motion blur angle 90°
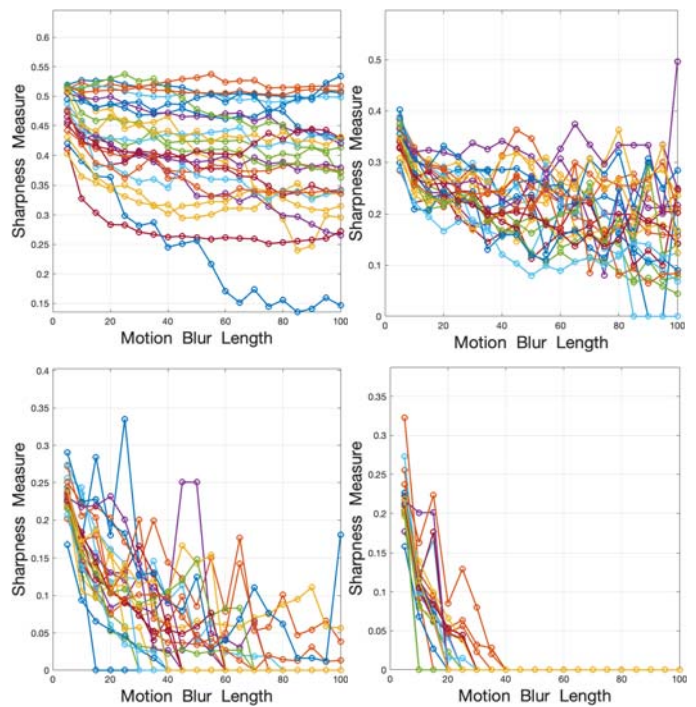

Fig. 11. Trend lines comparison: the variation of PSI [23] vs motion blur on Kodak 24 images. The top left corner: trend with a motion blur angle 0°. The top right: trend with a motion blur angle 30°. The bottom left: trend with a motion blur angle 60°. The bottom right: trend with a motion blur angle 90°
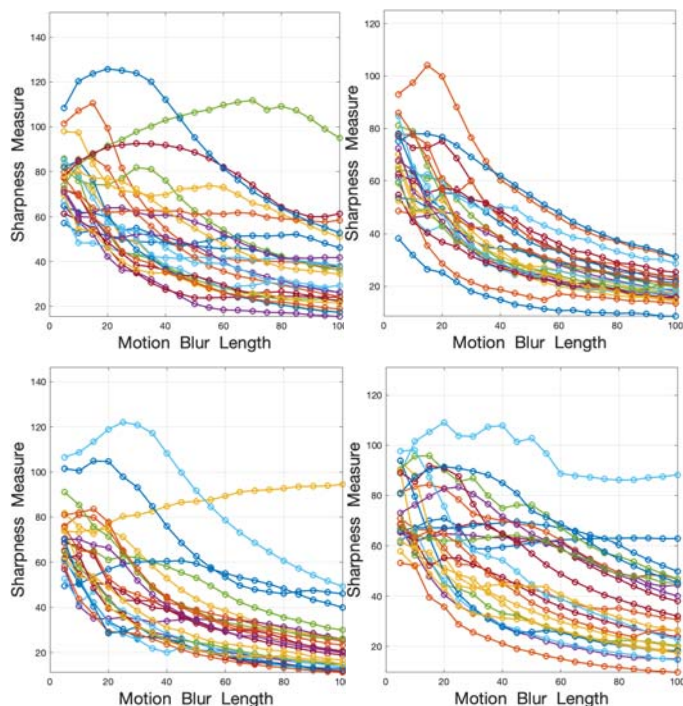
ISSN 2464-4617 (print)
ISSN 2464-4625 (online)

Computer Science Research Notes - CSRN 3401
http://www.wscg.eu

WSCG 2024
POSTERS

[7] Marziliano, Pina, et al. "Perceptual blur and ringing metrics: application to JPEG2000." Signal processing: Image communication 19.2 (2004): 163-172.

[8] Zhan, Yibing, and Rong Zhang. "No-reference image sharpness assessment based on maximum gradient and variability of gradients." IEEE Transactions on Multimedia 20.7 (2017): 1796-1808.

[9] Maini, Raman, and Himanshu Aggarwal. "Study and comparison of various image edge detection techniques." International journal of image processing (IJIP) 3.1 (2009): 1-11.

[10] Ahmed, Ahmed Shihab. "Comparative study among Sobel, Prewitt and Canny edge detection operators used in image processing." J. Theor. Appl. Inf. Technol 96.19 (2018): 6517-6525.

[11] Liu, Zhaoyang, et al. "An improved method for evaluating image sharpness based on edge information." Applied Sciences 12.13 (2022): 6712.

[12] De, Kanjar, and V. Masilamani. "Image sharpness measure for blurred images in frequency domain." Procedia Engineering 64 (2013): 149-158.

[13] Zhang, Zheng, et al. "Focus and blurriness measure using reorganized DCT coefficients for an autofocus application." IEEE Transactions on Circuits and Systems for Video Technology 28.1 (2016): 15-30.

[14] Tong, Hanghang, et al. "Blur detection for digital images using wavelet transform." 2004 IEEE international conference on multimedia and expo (ICME)(IEEE Cat. No. 04TH8763). Vol. 1. IEEE, 2004.

[15] Vu, Phong V., and Damon M. Chandler. "A fast wavelet-based algorithm for global and local image sharpness estimation." IEEE Signal Processing Letters 19.7 (2012): 423-426.

[16] Yitzhaky, Yitzhak, and Norman S. Kopeika. "Identification of blur parameters from motion blurred images." Graphical models and image processing 59.5 (1997): 310-320.

[17] Al Maki, Wikky Fawwaz, and Sueo Sugimoto. "Blind deconvolution algorithm for spatially-invariant motion blurred images based on inverse filtering and DST." International journal of circuits, systems and signal processing 1.1 (2007): 92-100.

[18] Chen, Xiaogang, et al. "Motion blur detection based on lowest directional high-frequency energy." 2010 IEEE International Conference on Image Processing. IEEE, 2010.

[19] Masaoka, Kenichiro, et al. "Modified slanted-edge method and multidirectional modulation transfer function estimation." Optics express 22.5 (2014): 6040-6046.

[20] Loebich, Christian, et al. "Digital camera resolution measurements using sinusoidal Siemens stars." Digital Photography III. Vol. 6502. SPIE, 2007.

[21] Cao, Frédéric, Frédéric Guichard, and Hervé Hornung. "Dead leaves model for measuring texture quality on a digital camera." Digital Photography VI. Vol. 7537. SPIE, 2010.

[22] Narvekar, Niranjan D., and Lina J. Karam. "A no-reference image blur metric based on the cumulative probability of blur detection (CPBD)." IEEE Transactions on Image Processing 20.9 (2011): 2678-2683.

[23] Feichtenhofer, Christoph, Hannes Fassold, and Peter Schallauer. "A perceptual image sharpness metric based on local edge gradient analysis." IEEE Signal Processing Letters 20.4 (2013): 379-382.

Fig. 12. Trend lines comparison: the variation of MGVG [8] vs motion blur on Kodak 24 images. The top left corner: trend with a motion blur angle 0°. The top right: trend with a motion blur angle 30°. The bottom left: trend with a motion blur angle 60°. The bottom right: trend with a motion blur angle 90°
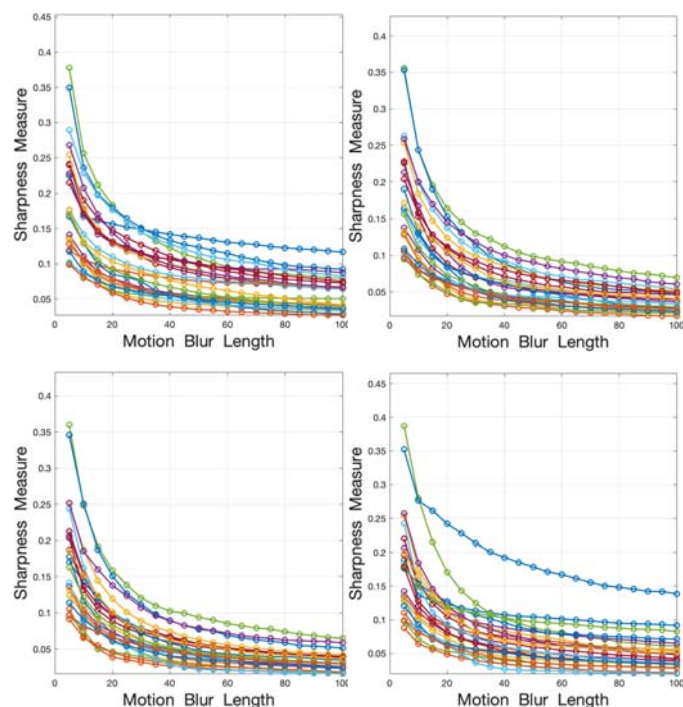

Fig. 13. Trend lines comparison: the variation of our proposed image quality metric of sharpness HFEM vs motion blur on Kodak 24 images. The top left corner: trend with a motion blur angle 0°. The top right: trend with a motion blur angle 30°. The bottom left: trend with a motion blur angle 60°. The bottom right: trend with a motion blur angle 90°